Source-Type Integral Equation Analysis of Circularly Curved Channel Waveguides in a Multilayered Background

Harrie J. M. Bastiaansen, H. Ed Crayé, and Hans Blok, *Member, IEEE*

***Abstract*—The source-type integral equation method has proven to be a powerful modeling tool for straight ridge waveguides. This method is full-vectorial and mathematically rigorous. In a previous publication the source-type integral equation method has also been successfully applied to circularly curved channel waveguides in a homogeneous background. In the present paper this approach is extended to circularly curved channel waveguides embedded in a multilayered background. These are the type of waveguide structures that are usually encountered in integrated-optical and optoelectronic devices.**

I. Introduction

OPTICAL WAVEGUIDES interconnect the various components present on an optoelectronic circuit. These circuits generally consist of a multilayered stack of dielectric materials, in which straight and curved channel waveguide tracks are made. The source-type integral equation method has already proven to be a powerful modeling tool for the determination of the guided modes of straight channel waveguides embedded in a multilayered background [1]–[3], and of curved channel waveguides embedded in a homogeneous background [4]. The method shows some resemblance with the Volume Current Method [5]–[8] but does not assume the electromagnetic field in the core of the waveguide to be known *à priori*.

In this paper, we complete the source-type integral equation analysis by focussing on the rigorous computation of the guided modes of circularly curved channel waveguides embedded in a multilayered background. The Green's tensor for the multilayered background is determined by a scattering-matrix formalism. Various numerical results are presented. In [4], [9], we have shown that considerable inaccuracies may occur when approximate methods like the Effective Index Method [10], [11] are applied to these waveguides. The full-vectorial, source-type integral equation method as presented in this paper does not show such inaccuracies.

The analysis presented in this paper completes the modal analysis for both straight and circularly curved planar and channel waveguides by means of a source-type integral equation. For a complete overview, see [12]. We have demonstrated that the source-type integral equation method can be a very powerful designing tool for optical waveguides.

Manuscript received September 1, 1994; revised January 19, 1995. This work was supported in part by the Stichting Fund for Science, Technology, and Research (a companion organization to the Schlumberger Foundation in the USA).

H. J. M. Bastiaansen, and H. E. Crayé are with the PTT Research, Dr. Neher Laboratory, Leidschendam, The Netherlands.

H. Blok is with the Department of Electrical Engineering, Delft University of Technology, Delft, The Netherlands.

IEEE Log Number 9412039.

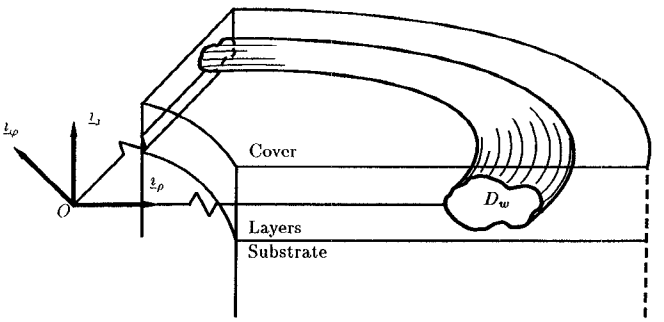

Fig. 1. The circularly curved channel waveguide embedded in a multilayered background.

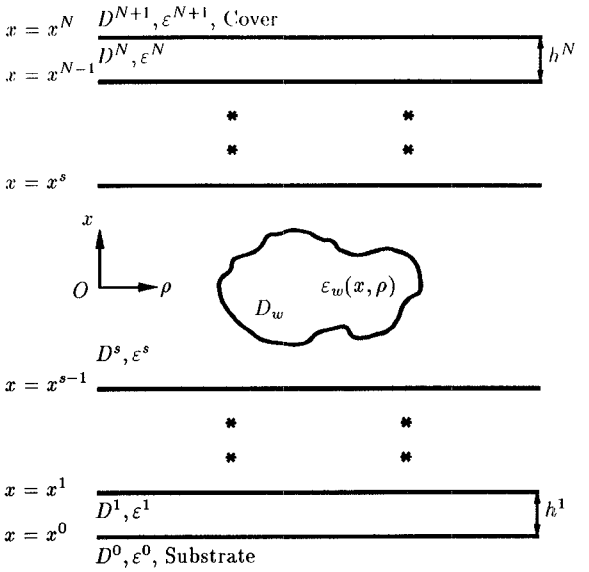

Fig. 2. Cross-section at fixed azimuthal φ-coordinate of the curved channel waveguide configuration.

II. Formulation of the Problem

The waveguiding structure we will investigate is the circularly curved channel waveguide embedded in a multilayered background (Figs. 1 and 2). A stack of N planar dielectric layers $D^1, D^2, \cdots, D^N$ is sandwiched between the semi-infinite substrate D^0 and the semi-infinite superstrate or cover D^{N+1}. The thickness of layer D^n is h^n, its

permittivity ε^n is real-valued (no losses assumed). Within layer D^s a circularly curved channel waveguide core $D_w, \rho_L < \rho < \rho_H, x_L(\rho) < x < x_H(\rho)$, with inhomogeneous permittivity profile $\varepsilon_w(x,\rho)$ is embedded. The right-handed cylindrical reference frame $\{O, \underline{i}_x, \underline{i}_\rho, \underline{i}_\varphi\}$ is introduced, such that the plane $x = 0$ is centered in D^s, i.e. it is equidistant to the planes $x = x^{s-1}$ and $x = x^s$. The channel waveguide core D_w is circularly curved around the axis $\rho = 0$. No 2π azimuthal periodicity of the electromagnetic fields is assumed.

In the waveguiding structure guided modes can propagate. These are time-harmonic solutions of the source-free Maxwell equations for which the electromagnetic field propagates harmonically and undeformed in the azimuthal φ-direction

$$\{\underline{\mathcal{E}}, \underline{\mathcal{H}}\}(x,\rho,\varphi;t) = \{\underline{E}, \underline{H}\}(x,\rho;k_\varphi)\exp[j(\omega t - k_\varphi \varphi)]. \quad (1)$$

In [4], a full-vectorial source-type integral equation has been derived to determine the guided modes for the case of a homogeneous background with permittivity ε_b

$$\begin{bmatrix} 1 & 0 & 0 \\ 0 & \frac{\varepsilon_w}{\varepsilon_b}(x,\rho) & 0 \\ 0 & 0 & 1 \end{bmatrix} \cdot \underline{E}(x,\rho;k_\varphi) = \frac{j\omega}{2\pi}\int_{-\infty}^{\infty} dk_x \iint_{D_w} [\varepsilon_w(x',\rho') - \varepsilon_b] \cdot \underline{\underline{G}}(x,\rho;x',\rho';k_x,k_\rho,k_\varphi) \cdot \underline{E}(x',\rho';k_\varphi)\rho'\, dx'\, d\rho' \quad (2)$$

with the Green's tensor $\underline{\underline{G}}$ equal to

$$\underline{\underline{G}} = \frac{\pi}{2\omega\varepsilon_b}\underline{\underline{\mathcal{G}}} J_{k_\varphi}(k_\rho\rho_<)H^{(2)}_{k_\varphi}(k_\rho\rho_>),$$

$$\rho_< = \min\{\rho,\rho'\}, \quad \rho_> = \max\{\rho,\rho'\},$$

$$\underline{\underline{\mathcal{G}}} = \left\{ \begin{bmatrix} -k_\rho^2 & -jS_x k_x \partial_{\rho'} & \frac{S_x k_x k_\varphi}{\rho'} \\ jS_x k_x \partial_\rho & -\frac{k_x^2}{k_\rho^2}\partial_\rho\partial_{\rho'} & \frac{-jk_x^2 k_\varphi}{k_\rho^2\rho'}\partial_\rho \\ \frac{S_x k_x k_\varphi}{\rho} & \frac{jk_x^2 k_\varphi}{k_\rho^2\rho}\partial_{\rho'} & \frac{-k_x^2 k_\varphi^2}{k_\rho^2\rho\rho'} \end{bmatrix} + \begin{bmatrix} 0 & 0 & 0 \\ 0 & \frac{-k_b^2 k_\varphi^2}{k_\rho^2\rho\rho'} & \frac{-jk_b^2 k_\varphi}{k_\rho^2\rho}\partial_{\rho'} \\ 0 & \frac{jk_b^2 k_\varphi}{k_\rho^2\rho'}\partial_\rho & -\frac{k_b^2}{k_\rho^2}\partial_\rho\partial_{\rho'} \end{bmatrix} \right\} \exp[jk_x|x'-x|] \quad (3)$$

and $S_x = \text{sign}(x'-x), k_b = \omega\sqrt{\varepsilon_b\mu_0}$, and $k_\rho = \sqrt{k_b^2 - k_x^2}$, $\text{Im}\{k_\rho\} \le 0$. For observation points (x,ρ) inside the channel waveguide core D_w, (2) constitutes a homogeneous Fredholm integral equation of the second kind. Non-trivial solutions exist for the values of the azimuthal wave number k_φ that are propagation constant of a guided mode. As radiation loss is inherent to the guided modes in curved waveguides, the propagation constants are complex valued. For modes propagating in the positive azimuthal direction, they are situated within the fourth quarter of the complex k_φ-plane. The value k_φ is represented through the effective refractive index N_{eff} (describing the phase velocity) and the radiation loss L_{rad}

$$N_{\text{eff}} = \text{Re}\{k_\varphi\}/(k_0\rho_H),$$
$$L_{\text{rad}} = -10\cdot\pi\cdot\text{Im}\{k_\varphi\}/\ln(10) \quad [\text{dB}/(90\text{ degrees})].$$

Equation (2) is reformulated by means of relation (19) of the Appendix as

$$\begin{bmatrix} \frac{\varepsilon_w}{\varepsilon_b}(x,\rho) & 0 & 0 \\ 0 & 1 & 0 \\ 0 & 0 & 1 \end{bmatrix} \cdot \underline{E}(x,\rho;k_\varphi) = -\frac{j\omega}{2\pi}\int_{-\infty}^{\infty}\frac{k_\rho}{k_x}dk_\rho \iint_{D_w} [\varepsilon_w(x',\rho') - \varepsilon_b] \cdot \underline{\underline{G}}(x,\rho;x',\rho';k_x,k_\rho,k_\varphi)\cdot\underline{E}(x',\rho';k_\varphi)\rho'\, dx'\, d\rho' \quad (4)$$

with $k_x = \sqrt{k_b^2 - k_\rho^2}$, $\text{Im}\{k_x\} \ge 0$, and the Green's tensor $\underline{\underline{G}}$ equal to

$$\underline{\underline{G}} = \frac{\pi}{2\omega\varepsilon_b}\underline{\underline{\mathcal{G}}} J_{k_\varphi}(k_\rho\rho)J_{k_\varphi}(k_\rho\rho').$$

The nonunity term on the diagonal of the matrix at the left-hand side has shifted from the $\rho\rho$-element of (2) to the xx-element of (4). This is due to the integral path deformation of the xx- and the $\rho\rho$-element of the Green's tensor for which $\alpha = -1$ (see Appendix).

The loss-free wave number k_b is considered as the limiting case of a lossy situation: $k_b = k_b - j0, \text{Re}\{k_b\} > 0$. Then, the definition of the complex root-function $k_x(k_\rho)$ shows that $k_x(k_\rho)$ is situated in the second quadrant of the complex plane. Therefore, the integral (4) directly shows that the boundary condition of exponentially decaying fields for $|x| \to \infty$ are satisfied. Hence, (4) will be used as the integral equation for the guided modes of the circularly curved channel waveguide in a multilayered background, for which the Green's tensor $\underline{\underline{G}}$ will be derived in the next section.

III. The Green's Tensor for the Multi-Layered Background

The p-column, $p = x,\rho,\varphi$, of the Green's tensor is the electric field, generated by an electric point-source situated within D^s and radiating in the direction of the unit vector $\underline{i}_p$. An azimuthal cross-section of the configuration for the point-source problem is shown in Fig. 3. The point-source divides layer D^s in D^{s-} and D^{s+}. The solution of the point-source problem is the superposition of two parts.

The primary part (superscript "*pri*") takes the inhomogeneity in Maxwell's equations due to the presence of the point-source into account. It is only non-vanishing within layer

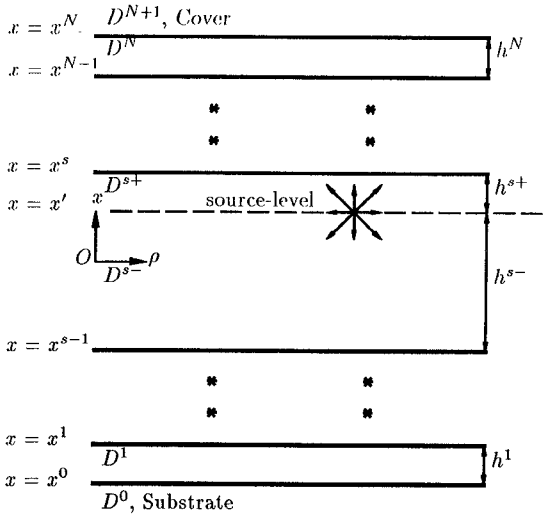

Fig. 3. Configuration for the point-source problem.

D^s where it equals the p-column of the Green's tensor (3) for the homogeneous background.

The secondary part (superscript "sec") satisfies the homogeneous Maxwell equations. It is defined within every layer of the background.

The construction of the solution of the point-source problem for the multilayered background is based on four relations:

General Solution: In D^n, the the general solution of the homogeneous Maxwell equations is [13, p. 91]:

$$\begin{aligned}\underline{E} =& \underline{\underline{\mathcal{E}}}(k_\rho, k_x^n) J_{k_\varphi}(k_\rho\rho) e^{\jmath k_x^n (x^{n,\mathrm{ref}} - x)} \cdot \underline{f}_p^{+,n} \\ &+ \underline{\underline{\mathcal{E}}}(k_\rho, -k_x^n) J_{k_\varphi}(k_\rho\rho) e^{-\jmath k_x^n (x^{n,\mathrm{ref}} - x)} \cdot \underline{f}_p^{-,n}, \\ \underline{H} =& \underline{\underline{\mathcal{H}}}(k_\rho, k_x^n) J_{k_\varphi}(k_\rho\rho) e^{\jmath k_x^n (x^{n,\mathrm{ref}} - x)} \cdot \underline{f}_p^{+,n} \\ &+ \underline{\underline{\mathcal{H}}}(k_\rho, -k_x^n) J_{k_\varphi}(k_\rho\rho) e^{-\jmath k_x^n (x^{n,\mathrm{ref}} - x)} \cdot \underline{f}_p^{-,n} \end{aligned} \quad (5)$$

with

$$\begin{aligned} k_x^n =& \sqrt{(k^n)^2 - k_\rho^2}, \mathrm{Im}\{k_x^n\} \geq 0, \\ \underline{f}_p^{\pm,n} =& (f_{p,E}^{\pm,n}, f_{p,H}^{\pm,n}), x^{n,\mathrm{ref}} = x^{n-1} \end{aligned}$$

if $n\epsilon\{s+, \cdots, N+1\}, x^{n,\mathrm{ref}} = x^n$ if $n\epsilon\{0, \cdots, s-\}$, and

$$\underline{\underline{\mathcal{E}}}(k_\rho, k_x^n) = \begin{bmatrix} 1 & 0 \\ \dfrac{-\jmath k_x^n}{k_\rho^2}\partial_\rho & \dfrac{\omega\mu_0 k_\varphi k_x^n}{k_\rho^2\rho} \\ \dfrac{-k_\varphi k_x^n}{k_\rho^2\rho} & \dfrac{-\jmath\omega\mu_0 k_x^n}{k_\rho^2}\partial_\rho \end{bmatrix},$$

$$\underline{\underline{\mathcal{H}}}(k_\rho, k_x^n) = \begin{bmatrix} 0 & -k_x^n \\ \dfrac{\omega\varepsilon^n k_\varphi}{k_\rho^2\rho} & \dfrac{\jmath(k_x^n)^2}{k_\rho^2}\partial_\rho \\ \dfrac{-\jmath\omega\varepsilon^n}{k_\rho^2}\partial_\rho & \dfrac{k_\varphi (k_x^n)^2}{k_\rho^2\rho} \end{bmatrix}.$$

Boundary Conditions: In D^0 and D^{N+1} the field must decay: $\underline{f}_p^{+,N+1} = \underline{f}_p^{-,0} = \underline{0}$.

Continuity Conditions: The continuous tangential field components in (5) are equated at the interfaces $x = x^n$, giving

$$\begin{bmatrix} \underline{f}_p^{+,n+1} \\ \underline{f}_p^{-,n+1} \end{bmatrix} = \underline{\underline{\mathcal{P}}}^{n+1\leftrightarrow n} \cdot \begin{bmatrix} \underline{f}_p^{+,n} \\ \underline{f}_p^{-,n} \end{bmatrix}.$$

The ij-element of $\underline{\underline{\mathcal{P}}}^{n+1\leftrightarrow n}$ vanishes if $i+j$ is odd.

Excitation Conditions: The unknown secondary vectors $\underline{f}_p^{\pm,s,\mathrm{sec}}$ are equal in D^{s+} and D^{s-}. The known primary vectors $\underline{f}_p^{\pm,s,\mathrm{pri}}$ differ. Elimination of $\underline{f}_p^{\pm,s,\mathrm{sec}}$ yields

$$\begin{aligned} \underline{f}_p^{+,s+} =& \underline{f}_p^{+,s-} + \underline{f}_p^{+,s+,\mathrm{pri}}, \\ \underline{f}_p^{-,s-} =& \underline{f}_p^{-,s+} + \underline{f}_p^{-,s-,\mathrm{pri}}. \end{aligned} \quad (6)$$

The solution of the point-source problem is uniquely determined by the boundary, continuity and excitation conditions. We will apply the scattering-matrix formalism to construct the solution. For this formalism, we refer to [14], in which it proved its effectiveness in the analysis of straight channel waveguides in a multilayered background. The formalism gives a recursive scheme for the determination of the reflection coefficients defined as

$$\begin{aligned} f_{p,i}^{-,n} =& r_i^{d,n} . f_{p,i}^{+,n}, \quad \text{if } n\epsilon\{s+, \cdots, N+1\}, \\ f_{p,i}^{+,n} =& r_i^{u,n} . f_{p,i}^{-,n}, \quad \text{if } n\epsilon\{0, \cdots, s-\}, \qquad i = E, H. \end{aligned} \quad (7)$$

The scattering-matrix formalism is a scalar recursive scheme independent of the p-value, $p = x, \rho, \varphi$, in which all exponentially increasing factors have been eliminated. Hence, it is both *numerically stable* and *efficient*.

It suffices to consider point-sources (x', ρ') and observation points (x, ρ) situated within D^s to determine the propagation constants k_φ of the guided modes. The reflection coefficients $r_i^{d,s+}$ and $r_i^{u,s-}$ are expressed in the reflection coefficients r_i^{d*} and r_i^{u*} of a point-source situated at the center $x' = 0$ of D^s through $r_i^{d,s+}(x') = \exp[-2\jmath k_x^s x'] r_i^{d*}, r_i^{u,s-}(x') = \exp[2\jmath k_x^s x'] r_i^{u*}$. With the reflection coefficients, (5) yields the electric field generated by the point-source and hence the p-column of the Green's tensor. For $(x, \rho)\epsilon D^s$, the Green's tensor $\underline{\underline{G}}$ multilayered background for the source-type integral (4) becomes

$$\underline{\underline{G}} = -\frac{k_\rho}{k_x^s}\frac{\pi}{2\omega\varepsilon^s}\underline{\underline{\mathcal{G}}}(x, \rho; x', \rho'; k_x, k_\rho, k_\varphi) J_{k_\varphi}(k_\rho\rho) J_{k_\varphi}(k_\rho\rho'),$$

$$\underline{\underline{\mathcal{G}}} = \begin{bmatrix} -ak_\rho^2 & -bjk_x^s S_x \partial_{\rho'} & b\dfrac{k_x^s k_\varphi S_x}{\rho'} \\ cjk_x^s S_x \partial_\rho & -d\dfrac{(k_x^s)^2}{k_\rho^2}\partial_\rho\partial_{\rho'} & -d\dfrac{j(k_x^s)^2 k_\varphi}{k_\rho^2\rho'}\partial_\rho \\ c\dfrac{k_x^s k_\varphi S_x}{\rho} & d\dfrac{j(k_x^s)^2 k_\varphi}{k_\rho^2\rho}\partial_{\rho'} & -d\dfrac{(k_x^s)^2 k_\varphi^2}{k_\rho^2\rho\rho'} \end{bmatrix} + \begin{bmatrix} 0 & 0 & 0 \\ 0 & -e\dfrac{(k^s)^2 k_\varphi^2}{k_\rho^2\rho\rho'} & -e\dfrac{j(k^s)^2 k_\varphi}{k_\rho^2\rho}\partial_{\rho'} \\ 0 & e\dfrac{j(k^s)^2 k_\varphi}{k_\rho^2\rho'}\partial_\rho & -e\dfrac{(k^s)^2}{k_\rho^2}\partial_\rho\partial_{\rho'} \end{bmatrix}, \quad (8)$$

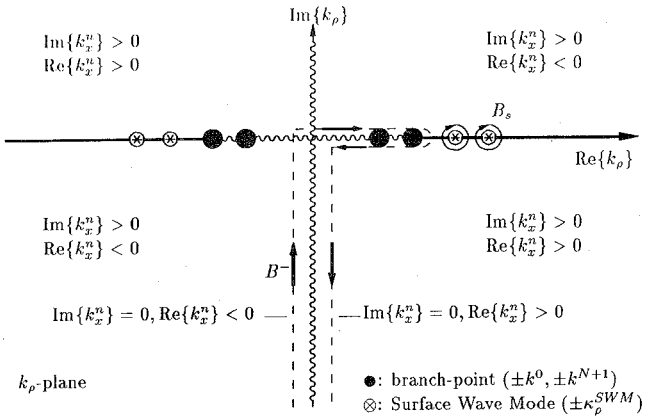

Fig. 4. Deformation of the path of integration in the k_ρ-plane.

$$\left.\begin{aligned}
a &= \exp[jk_x^s(x'-x)](\exp[2jk_x^s x] + r_E^{d*}) \\
&\quad \cdot (\exp[-2jk_x^s x'] + r_E^{u*})/(1 - r_E^{d*} r_E^{u*}), \\
b &= \exp[jk_x^s(x'-x)](\exp[2jk_x^s x] + r_E^{d*}) \\
&\quad \cdot (\exp[-2jk_x^s x'] - r_E^{u*})/(1 - r_E^{d*} r_E^{u*}), \\
c &= \exp[jk_x^s(x'-x)](\exp[2jk_x^s x] - r_E^{d*}) \\
&\quad \cdot (\exp[-2jk_x^s x'] + r_E^{u*})/(1 - r_E^{d*} r_E^{u*}), \\
d &= \exp[jk_x^s(x'-x)](\exp[2jk_x^s x] - r_E^{d*}) \\
&\quad \cdot (\exp[-2jk_x^s x'] - r_E^{u*})/(1 - r_E^{d*} r_E^{u*}), \\
e &= \exp[jk_x^s(x'-x)](\exp[2jk_x^s x] - r_H^{d*}) \\
&\quad \cdot (\exp[-2jk_x^s x'] - r_H^{u*})/(1 - r_H^{d*} r_H^{u*}),
\end{aligned}\right\} \quad x > x',$$

$$\left.\begin{aligned}
a &= \exp[jk_x^s(x-x')](+\exp[-2jk_x^s x] + r_E^{u*}) \\
&\quad \cdot (+\exp[2jk_x^s x'] + r_E^{d*})/(1 - r_E^{d*} r_E^{u*}), \\
b &= \exp[jk_x^s(x-x')](+\exp[-2jk_x^s x] + r_E^{u*}) \\
&\quad \cdot (-\exp[2jk_x^s x'] + r_E^{d*})/(1 - r_E^{d*} r_E^{u*}), \\
c &= \exp[jk_x^s(x-x')](-\exp[-2jk_x^s x] + r_E^{u*}) \\
&\quad \cdot (+\exp[2jk_x^s x'] + r_E^{d*})/(1 - r_E^{d*} r_E^{u*}), \\
d &= \exp[jk_x^s(x-x')](-\exp[-2jk_x^s x] + r_E^{u*}) \\
&\quad \cdot (-\exp[2jk_x^s x'] + r_E^{d*})/(1 - r_E^{d} r_E^{u*}), \\
e &= \exp[jk_x^s(x-x')](-\exp[-2jk_x^s x] + r_H^{u*}) \\
&\quad \cdot (-\exp[2jk_x^s x'] + r_H^{d*})/(1 - r_H^{d*} r_H^{u*}),
\end{aligned}\right\} \quad x < x'.$$

Relation (19) in the Appendix shows that the Green's tensor can as well be expressed in terms of the Hankel function as

$$\underline{\underline{G}} = -\frac{k_\rho}{k_x^s}\frac{\pi}{2\omega\varepsilon}\underline{\underline{\mathcal{G}}}(x,\rho;x',\rho';k_x,k_\rho,k_\varphi) \cdot H_{k_\varphi}^{(2)}(k_\rho\rho_>)J_{k_\varphi}(k_\rho\rho_<). \tag{9}$$

From a numerical point of view, the inverse transformation of the radial wave number k_ρ over the real axis is not very attractive as the Bessel and Hankel functions are strongly oscillating and have to be computed with the complicated and CPU-time consuming Nicholson's expansion [15, 9.3.35–9.3.46]. Therefore, deformation of the integral path is applied. This requires that the branch-points and pole singularities of the Green's tensors for the multilayered background in the complex k_ρ-plane are identified (Fig. 4).

Branch-Points. The root function $k_x^n = \sqrt{(k^n)^2 - k_\rho^2}$ has branch-points $k_\rho = \pm k^n$ and branch-cuts $\mathrm{Im}\{k_x^n\} = 0$. For layers D^n in between the substrate and the cover the components of the Green's tensor $\underline{\underline{G}}$ are even functions of k_x^n and the branch-points vanish.

Pole Singularities. These are the discrete points for which the term $1 - r_i^{d*} r_i^{u*}$ vanishes. For these k_ρ-values, the background supports non-trivial solutions of the homogeneous Maxwell-equations, i.e. the pole singularities are the guided modes of the planar multilayered background. The pole singularities are situated on the real k_ρ-axis.

The integration path is deformed from the real k_ρ-axis into the branch-cut B^-, complemented with the contours B_s, each enclosing a pole singularity. The non-unity term in the left-hand side of (4) reshifts from the xx-element to the $\rho\rho$-element (see Appendix for $\alpha = -1$). For k_ρ on B^-, the Bessel and Hankel functions do not oscillate but behave as exponentially decaying functions. Over almost the complete range, they can easily be evaluated with Debye's expansion [15, 9.3.7–9.3.14].

IV. Numerical Implementation

To convert the continuous source-type integral equation into its discrete counterpart suitable for numerical solution, the method of moments is applied [16]. The electric field $\underline{E}(x,\rho)$ is expanded into a summation of expansion functions $f_l(x,\rho)$

$$\underline{E}(x,\rho) = \sum_{l=1}^{L} f_l(x,\rho)\underline{E}_l, \qquad (x,\rho)\epsilon D_w. \tag{10}$$

Subsequently, the weighting procedure with weighting functions $w_m(x,\rho)$ is applied over the cross-section of the waveguide. A set of $3 \times L$ linear algebraic equations for the $3 \times L$ components of the expansion vectors $\underline{E}_l$ results

$$\sum_{l=1}^{L} \underline{\underline{L}}_{m;l} \cdot \underline{E}_l = -\frac{j\omega}{2\pi}\sum_{l=1}^{L} \cdot \left(\int_{B^-} + \sum\int_{B_s}\right)\frac{k_\rho}{k_x^s}\underline{\underline{R}}_{m;l}(k_\rho,k_\varphi)\,dk_\rho \cdot \underline{E}_l, \quad m\epsilon\{1,\cdots,L\} \tag{11}$$

in which

$$\underline{\underline{L}}_{m;l} = \iint_{D_w} \begin{bmatrix} 1 & 0 & 0 \\ 0 & \dfrac{\varepsilon_w(x,\rho)}{\varepsilon_b} & 0 \\ 0 & 0 & 1 \end{bmatrix} w_m(x,\rho) f_l(x,\rho)\,dx\,d\rho,$$

$$\underline{\underline{R}}_{m;l}(k_\rho,k_\varphi) = \iint_{D_w} w_m(x,\rho)\,dx\,d\rho \iint_{D_w} \cdot [\varepsilon_w(x',\rho') - \varepsilon_b]\underline{\underline{G}}(x,\rho;x',\rho';k_\rho,k_\varphi) \cdot f_l(x',\rho')\rho'\,dx'\,d\rho'.$$

Relation (11) is the discrete form of the source-type integral equation. It constitutes a system of $3 \times L$ homogeneous linear equations that can be represented as

$$\underline{\underline{A}}(k_\varphi) \cdot \underline{X} = \underline{0} \tag{12}$$

in which the overall expansion vector $\underline{X}$ contains the individual expansion vectors $\underline{E}_l$. A non-trivial solution exists only if the determinant of the system is equal to zero

$$\det[\underline{\underline{A}}(k_\varphi)] = 0. \tag{13}$$

The propagation constants k_φ of the guided modes fulfill (13). Condition (13) is the resonance condition for the source-type

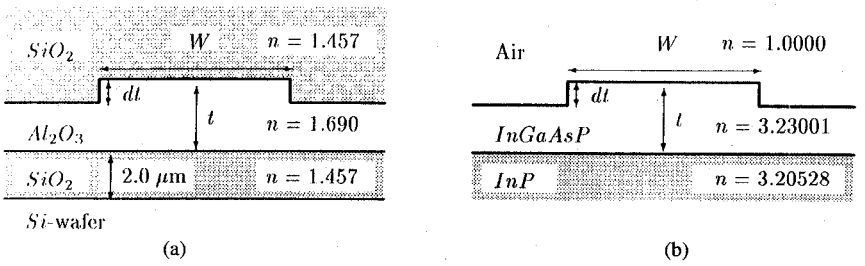

Fig. 5. COST 216 waveguide configurations: (a) strongly guiding waveguide configuration, (b) weakly guiding waveguide configuration.

integral method. If a propagation constant and its overall expansion vector $\underline{X}$ have been determined, (10) gives the electric field distribution inside D_w and, subsequently, the integral representation (4) gives the electric field distribution outside D_w as well. The magnetic field follows by applying the curl-operation to the electric field. The complex zeros of the resonance condition (13) within a contour in the complex k_φ-plane are evaluated with the method presented by Delves and Lyness [17].

In view of the applications in optoelectronic devices, we restrict ourselves to homogeneous rectangular channel waveguide cores D_w

$$D_w: \quad -\frac{h}{2} \le x \le \frac{h}{2}, \quad \rho_L \le \rho \le \rho_H, \quad \varepsilon_w(x,\rho) = \varepsilon_w.$$

An efficient algorithm to evaluate the k_ρ-integrations over B^- (11) has been outlined in [4]. This algorithm is shortly recapitulated here. Separable expansion and weighting functions are chosen

$$\left.\begin{aligned} f_l(x,\rho) &= f_p^\rho(\rho) f_q^x(x), \\ w_l(x,\rho) &= w_p^\rho(\rho) w_q^x(x), \end{aligned}\right\}$$
$$p\epsilon\{1,\cdots,P\},$$
$$q\epsilon\{1,\cdots,Q\},$$
$$P \times Q = L. \tag{14}$$

The integrand for the k_ρ-integrations over B^- is separated in a k_φ-dependent part (i.e. the ρ,ρ'-dependence), and a k_φ-independent part (i.e. the x,x'-dependence). Next, the integration path B^- is divided into J_r and J_i intervals on the real and imaginary axis, respectively. On each interval, the k_φ-dependent part of the integrand is approximated by a summation of K Chebyshev polynomials with k_φ-dependent weight-factors. For each Chebyshev polynomial and interval, the k_ρ-integration over the remaining k_φ-independent integrand is evaluated, and the result is stored. All k_ρ-integrations over B^- for subsequent k_φ-values reduce into a mere determination of the k_φ-dependent weight-factors of the Chebyshev polynomials for the k_φ-dependent part of the integrand, followed by a summation of the already stored results for the remaining k_φ-independent integrations. This numerical algorithm operates very efficiently. However, it poses some restrictions on the choice of the expansion and weighting functions. Hence, as in [4] we take adapted cubic B-splines and Dirac functions as expansion and weighting functions in the ρ-direction. In the x-direction equidistant triangle and pulse functions are chosen as expansion functions and weighting functions, respectively. The spatial integrations in the x-direction are performed analytically, those in the ρ-direction are performed numerically using Gaussian quadrature. To obtain high accuracy of the numerical results, the various discretization parameters are set as $J_r = 2$, $J_i = 6$, $K = 15$, $P = 16$, $Q = 4$.

TABLE I
THE EFFECTIVE REFRACTIVE INDEX N_{eff} AND THE RADIATION LOSS L_{rad} OF THE TE_{00}-MODE AND THE TM_{00}-MODE FOR THE STRONGLY GUIDING COST-WAVEGUIDE VERSUS THE RADIUS ρ_H

	TE_{00}			TM_{00}	
	STIM		EIM	STIM	
ρ_H	N_{eff}	L_{rad}	L_{rad}	N_{eff}	L_{rad}
20 μm	1.529345	15.039	15.528	1.510267	15.201
40 μm	1.540401	3.2452	3.7468	1.520892	3.668
60 μm	1.545567	0.4237	0.4377	1.525822	0.850
80 μm	1.548928	0.0376	0.0389	1.528935	0.093
100 μm	1.551314	0.0027	0.0028	1.531243	0.005
500 μm	1.562330	0.0000	0.0000	1.541923	0.000
1000 μm	1.564500	0.0000	0.0000	1.544050	0.000
2500 μm	1.565976	0.0000	0.0000	1.545503	0.000
5000 μm	1.566500	0.0000	0.0000	1.546019	0.000
∞	1.567041	0.0000	0.0000	1.546551	0.000

V. NUMERICAL RESULTS

The first numerical example of the source-type integral equation method (STIM) is the strongly guiding configuration Fig. 5(a), as studied in the COST 216 project [18] (COST: European Cooperation in the Field of Scientific and Technical Research). The dimensions of the ridge and background are: $W = 3.5$ μm, $t = 0.24$ μm and $dt = 0.1$ μm. The operating free-space wavelength is $\lambda_0 = 0.6328$ μm. In Table I, both the effective refractive index and the radiation loss for the strongly guiding waveguide configuration are presented as a

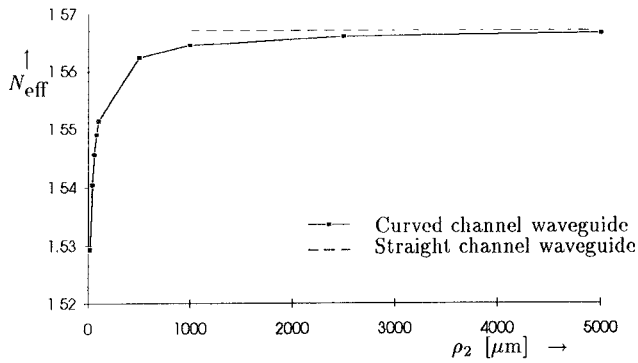

Fig. 6. The effective refractive index N_{eff} of the TE_{00}-mode of the strongly guiding COST-waveguide versus the radius ρ_H.

TABLE II
THE EFFECTIVE REFRACTIVE INDEX N_{eff} AND THE RADIATION LOSS L_{rad} OF THE TE_{00}-MODE FOR THE WEAKLY GUIDING COST-WAVEGUIDE VERSUS THE RADIUS ρ_H

weakly guiding: TE_{00}		
ρ_H	STIM	EIM
24000 μm	4.2414	0.0850
20000 μm	9.1567	0.3955
16000 μm	18.473	1.7278

function of the radius ρ_H. To test the consistency of the STIM for curved channel waveguides with that of straight channel waveguides [14], the results for the straight channel waveguide have been included ($\rho_H = \infty$) as well. The data of Table I for the effective refractive index of the TE_{00}-mode are graphically presented in Fig. 6. For $\rho_H \to \infty$, the effective refractive index of the curved channel waveguide configuration converges to that of the straight channel waveguide configuration. A similar behavior can be observed for the TM_{00}-mode.

For the TE_{00}-mode the radiation loss as computed with the well-known approximate Effective Index Method (EIM) has been included in Table I as well. If one compares the results of the STIM and the EIM, the differences seem to be marginal, and the effort in deriving the STIM does not seem justified. This changes however if one considers the weakly guiding waveguide COST-configuration of Fig. 5(b), with dimensions $W = 2.0$ μm, $t = 1.3$ μm and $dt = 0.3$ μm. The operating free-space wavelength is $\lambda_0 = 1.286$ μm. In Table II, the radiation loss of the TE_{00}-mode is given as function of the radius ρ_H. The radiaton loss as found with the STIM differs considerably from that found with the EIM. A factor more than 10 in Decibel radiation loss is observed for radii above 16 000 μm. Even larger differences between the results of the EIM and the STIM were observed for other waveguide configurations [9].

Subsequently, we compare the results of the STIM with the results of the semi-vectorial Method of Lines (MoL), as presented by Gu in his thesis [19]. Experimental results for the configuration are available as well. The configuration is

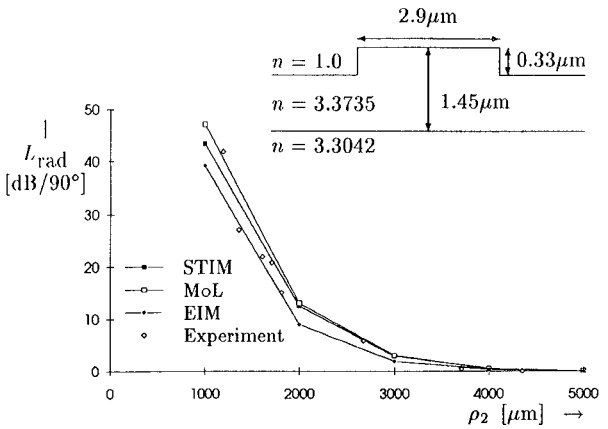

Fig. 7. The radiation loss L_{rad} of the TE_{00}-mode of the Deri-waveguide versus the radius ρ_H.

TABLE III
THE EFFECTIVE REFRACTIVE INDEX N_{eff} AND THE RADIATION LOSS L_{rad} OF THE TE_{00}-MODE AND THE TM_{00}-MODE FOR THE DERI-WAVEGUIDE VERSUS THE RADIUS ρ_H

	TE_{00}		TM_{00}	
ρ_H	N_{eff}	L_{rad}	N_{eff}	L_{rad}
1000 μm	3.341897	43.2323	3.339708	28.8042
2000 μm	3.343488	12.4522	3.341286	4.8828
3000 μm	3.344056	2.9519	3.341890	0.6013
4000 μm	3.344369	0.5915	3.342224	0.0630
5000 μm	3.344571	0.1065	3.342436	0.0075

the GaAs/AlGaAs optical rib waveguide of Deri *et al.* [20]. The description of the configuration is enclosed as inset in Fig. 7. The waveguide is operated at the free-space wavelength $\lambda_0 = 1.52$ μm. The effective refractive index and the radiation loss for the TE_{00}-mode and the TM_{00}-mode are given in Table III. For the TE_{00}-mode, the radiation loss is graphically presented in Fig. 7. The results of the EIM, the MoL and the experimental results have been included as well.

The source-type integral equation presented in this paper is full-vectorial. Field-plots of the components E_x, E_ρ and E_φ can be obtained. These field-components are complex-valued. Fig. 8 shows their norm for the TE_{00}-mode for the Deri waveguide configuration for the outer radius $\rho_H = 3000.0$ μm, together with the field-intensity $|\underline{E}|$. The outward shift of the field-distribution due to the waveguide curvature is clearly visible.

VI. CONCLUSION

The full-vectorial and mathematically rigorous source-type integral equation analysis has been extended to circularly curved channel waveguides with arbitrary cross-section embedded in a multilayered background. Numerical results for a broad range of curved channel waveguide configurations

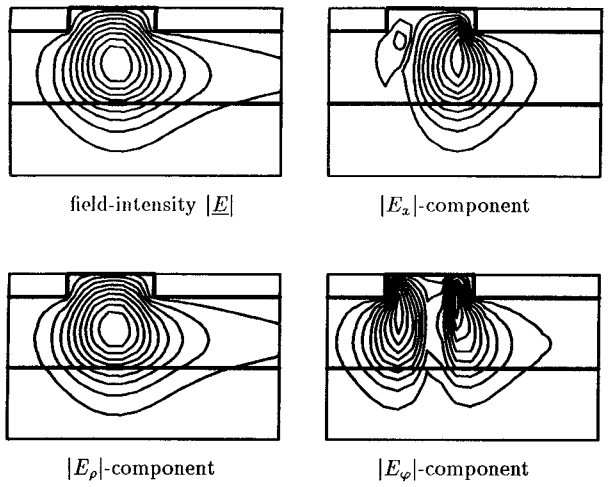

Fig. 8. Field-distribution of the TE_{00}-mode for the Deri waveguide at $\rho_H = 3000.0$ μm.

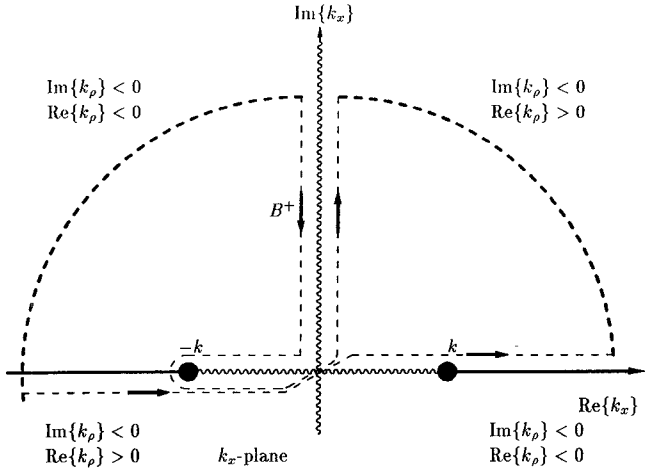

Fig. 9. Deformation of the path of integration in the k_x-plane.

have been presented. The results of the source-type integral method have been compared with experimental results and numerical results of other methods (especially the Effective Index Method). Considerable disagreements were observed for some configurations. For a more complete overview of the source-type integral equation method and a multitude of numerical results, the reader is referred to [12].

APPENDIX

For $\nu \epsilon C, \mathrm{Re}\{\nu\} \geq 0$, and $k_\rho = \sqrt{k^2 - k_x^2}, \mathrm{Im}\{k_\rho\} \leq 0$, the integral I is defined as

$$I := \int_{-\infty}^{\infty} f(k_x, k_\rho) J_\nu(k_\rho \rho_<) H_\nu^{(2)}(k_\rho \rho_>) \cdot \exp[jk_x|x' - x|]\, dk_x. \tag{15}$$

Let $f(k_x, k_\rho)$ be an analytic function of k_x and an even analytic function of k_ρ. Then $f(k_x, k_\rho(k_x))$ has the branch-cut $B^+, \mathrm{Im}\{k_\rho\} = 0$, see Fig. 9. Furthermore, let $f(k_x, k_\rho) = O(k_x^\alpha), |k_x| \to \infty$, for $\alpha < -1$. Then, the large argument expansion of the Bessel and Hankel function shows that integral path deformation from $k_x \epsilon R$ into the contour around the branch-cut B^+ is allowed. Change of integration variable from k_x to k_ρ yields

$$I = -\int_{-\infty}^{\infty} \frac{k_\rho}{k_x} f(k_x, k_\rho) J_\nu(k_\rho \rho_<) H_\nu^{(2)}(k_\rho \rho_>) \cdot \exp[jk_x|x' - x|]\, dk_\rho. \tag{16}$$

As $H_\nu^{(2)} = 2J_\nu - H_\nu^{(1)}$ we find $I = 2I_1 - I_2$ with

$$I_1 = -\int_{-\infty}^{\infty} \frac{k_\rho}{k_x} f(k_x, k_\rho) J_\nu(k_\rho \rho) J_\nu(k_\rho \rho') \cdot \exp[jk_x|x' - x|]\, dk_\rho, \tag{17}$$

$$I_2 = -\int_{-\infty}^{\infty} \frac{k_\rho}{k_x} f(k_x, k_\rho) J_\nu(k_\rho \rho_<) H_\nu^{(1)}(k_\rho \rho_>) \cdot \exp[jk_x|x' - x|]\, dk_\rho. \tag{18}$$

With change of integration variable $k_\rho \to -k_\rho$ in (18) and $H_\nu^{(1)}(-z) = -e^{-\nu\pi j} H_\nu^{(2)}(z), J_\nu(-z) = e^{\nu\pi j} J_\nu(z)$ and $f(k_x, -k_\rho) = f(k_x, k_\rho)$ we find

$$I = I_1 = I_2. \tag{19}$$

Similar relations hold for the derivatives of the Bessel and Hankel functions.

Note: If $\alpha = -1$, the non-uniform convergence of (15) for $\rho = \rho'$ gives rise to additional terms when deformation of the path of integration is applied.

REFERENCES

[1] J. Sader, "Analysis of arbitrarily perturbed circular profiles by implementation of integral-equation theory," *J. Opt. Soc. Amer. A*, vol. 7, no. 11, pp. 2094–2099, Nov. 1990.

[2] F. Olyslager and D. de Zutter, "Rigorous boundary integral solution for general isotropic and uniaxial anisotropic dielectric waveguides in multilayered media including losses, gain and leakage," *IEEE Trans. Microwave Theory Tech.*, vol. 41, no. 8, pp. 1385–1392, 1993.

[3] E. Kolk, N. Baken, and H. Blok, "Domain-integral equation analysis of integrated-optical channel and ridge waveguides in stratified media," *IEEE Trans. Microwave Theory Tech.*, vol. 38, no. 1, pp. 78–85, Jan. 1990.

[4] H. Bastiaansen, M. van der Keur, and H. Blok, "Full-vectorial source-type integral equation analysis of circularly curved channel waveguides," *IEEE Trans. Microwave Theory Tech.*, Feb. 1995.

[5] P. Kendall, J. Marsh, P. Robson, and R. Hewson-Browne, "Fraunhofer interference of a dielectric interface with travelling wave radiation and the consequent reduction in dielectric waveguide bending loss," *IEEE Proc.*, vol. 132-J, no. 6, pp. 354–358, Dec. 1985.

[6] P. Kendall, P. Robson, and E. Sitch, "Rib waveguide curvature loss: The scalar problem," *IEEE Proc.*, vol. 132-J, no. 2, pp. 140–145, Apr. 1985.

[7] P. Kendall, M. Stern, and P. Robson, "Huygens-type formula for curvature loss from dielectric waveguides in optoelectronics," *Electron. Lett.*, vol. 23, no. 16, pp. 850–851, July 1987.

[8] T. Benson, P. Kendall, and M. Stern, "Microwave simulation of opto-electronic bending loss in presence of dielectric discontinuity," *IEEE Proc.*, vol. 135-J, no. 4, pp. 325–329, Aug. 1988.

[9] H. Bastiaansen, J. van der Tol, and D. van den Berge, "Comment on article by Jaeger and Lai, accepted for publication," *Appl. Opt.*, 1994.

[10] E. Pennings, "Bends in optical ridge waveguide, modeling and experiments," Ph.D. thesis, University of Technology Delft, The Netherlands, ISBN: 90-9003413-7, June 1990.

[11] C. Vassallo, *Optical Waveguide Concepts*. Amsterdam: Elsevier, 1991.

[12] H. Bastiaansen, "Modal analysis of straight and curved integrated optical waveguides; An integral equation approach," Ph.D. thesis, University of Technology Delft, The Netherlands, ISBM: 90-72125-41-X, Dec. 1994.

[13] L. Lewin, D. Chang, and E. Kuester, "Electromagnetic waves and curved structures," *IEEE Electromagn. Waves Series 2*, J. R. Wait *et al.*, Eds. Stevenage, UK: Peregrinus, 1977.

[14] H. Bastiaansen, N. baken, and H. Blok, "Domain-integral analysis of channel waveguides in anisotropic multilayered media," *IEEE Trans. Microwave Theory Tech.*, vol. 40, no. 10, pp. 1918–1926, Oct. 1992.
[15] M. Abramowtic and I. Stegun, *Handbook of Mathematical Functions*. New York: Dover, 1965.
[16] R. Harrington, "The method of moments in electromagnetics," *J. Electromagn. Waves Applicat.*, vol. 1, no. 3, pp. 181–200, 1987.
[17] L. Delves and J. Lyness, "A numerical method for locating the zeros of an analytic function," *Math. Comput.*, vol. 21, pp. 543–560, 1967.
[18] P. Lagasse *et al.*, "Cost-216 comparative study of S-bend and directional coupler analysis methods," in *ECOC Conf. Publ.*, Sept. 1990.
[19] J. Gu, "Numerical analysis of directionally varying optical waveguides," Ph.D. thesis, Swiss Federal Institute of Technology, Zürich, 1991.
[20] R. Deri and R. Hawkins, "Polarization, scattering and coherent effects in semiconductor rib waveguide bends," *Opt. Lett.*, vol. 13, no. 10, pp. 922–924, Oct. 1988.

Harrie J. M. Bastiaansen was born in Tilburg, the Netherlands, on May 10, 1965. He received his M.Sc. degree in mathematics, cum laude, from the Eindhoven University of Technology in 1988, having specialized in the mechanics of rigid bodies.

In 1989, he became member of the scientific staff of the PTT Dr. Neher Laboratories, Leidschendam, The Netherlands. Initially, his interest has been in the guided wave characteristics of passive channel waveguide structures. As such, he has finished his Ph.D. thesis on the integral equation analysis of the guided modes in straight and curved channel waveguides in December 1994. Presently, he is involved in studies on the impact of advanced broadband transmission techniques on the telecommunications infrastructure and is actively involved in the European EURESCOM project: Overall Strategic Studies.

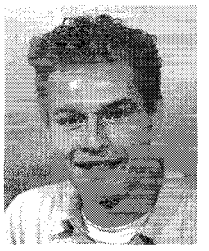

H. Ed Crayé was born in Amsterdam, The Netherlands, on July 5, 1972. In 1990 he started his study in electrical engineering at the Delft University of Technology.

In that same year, he became a Member of the Laboratory of Electromagnetic Research at the Delft University of Technology. Presently, at the final stage in his study, he is working at the PTT Dr. Neher Laboratories, Leidschendam, The Netherlands, where he is assisting with the numerical implementation of the full-vectorial source-type integral equation method for straight as well as circularly curved channel waveguides.

Hans Blok (M'87) was born in Rotterdam, The Netherlands, on April 14, 1935. He received the degree in electrical engineering from the Polytechnical School of Rotterdam in 1956. Het then received the B.Sc. and M.Sc. degrees in electrical engineering and the Ph.D. degree in technical sciences, all form the Delft University of Technology, in 1961, 1963, and 1970 respectively.

Since 1968, he has been a Member of the Scientific Staff of the Laboratory of Electromagnetic Research at the Delft University of Technology. During these years, he has carried out research and lectured in the areas of signal processing, wave propagation, and scattering problems. During the academic year 1970–1971, he was a Royal Society Research Fellow in the Department of Electronics of the University of Southampton, U.K., where he was involved in experimental and theoretical research on lasers and nonlinear optics. In 1972 he was appointed Associate Professor at the Delft University of Technology, and in 1980 he was named Professor. From 1980 to 1982 he was dean of the Faculty of Electrical Engineering. During the academic year 1983-1984 he was visiting scientist at Schlumberger-Doll Research, Ridgefield, CT. At present, his main research interest is in guided wave optics and inverse scattering problems.